Determination of neutron and proton multipole matrix elements in ^{208}Pb from π^- and π^+ scattering at 180 MeV

N. M. Hintz,[1] X. H. Yang,[1] M. Gazzaly,[1] S. J. Seestrom-Morris,[2] C. L. Morris,[2] D. C. Cook,[1] A. M. Mack,[1] J. W. McDonald,[3] S. Mordechai,[3,*] D. S. Oakley,[3,†] C. F. Moore,[3] M. Lynker,[3] and J. D. Zumbro,[4,‡]

[1]*University of Minnesota, Minneapolis, Minnesota 55455*

[2]*Los Alamos National Laboratory, Los Alamos, New Mexico 87545*

[3]*University of Texas, Austin, Texas 78712*

[4]*University of Pennsylvania, Philadelphia, Pennsylvania 19104*

(Received 16 April 1991)

New data for elastic and inelastic π^+ and π^- scattering by ^{208}Pb at 180 MeV are presented. The elastic scattering data were analyzed with a standard Kisslinger potential in a coordinate space (r space) calculation using the free π-N amplitudes to calculate the potential coefficients. Momentum-space (p-space) calculations were also performed using the free π-N amplitudes to calculate on-shell matrix elements and the Landau-Tabakin model for the off-shell. The same ground-state proton and neutron densities were used in these two spaces and the fits are good. The distorted-wave impulse approximation calculations in both spaces, with the same collective model transition densities, reproduce the inelastic differential cross sections quite well. The proton and neutron transition multipole matrix elements and their ratios were calculated from the deformation parameters extracted from fits to inelastic scattering data. It is found that the ratios calculated in these two spaces are quite close to each other and close to those found in a comparison of (e,e') and (p,p') experiments, while the absolute value of matrix elements found in the p-space calculations are $\sim$15–20 % smaller than those from the r-space calculations. The r-space proton matrix elements are generally in good agreement with those obtained from electron scattering. The effects of the pion-nucleon interactions and form factors used in these calculations were investigated.

PACS number(s): 25.80.Dj, 25.80.Ek, 23.20.Js, 27.80.+w

I. INTRODUCTION

The determination of neutron and proton multipole matrix elements M_n and M_p for inelastic transitions has been the subject of continuing interest in experimental and theoretical studies over the past several years [1–5]. These matrix elements provide a good test of different nuclear models. Their magnitudes and ratios have been studied extensively by comparing (p,p') with (e,e') scattering. Because of the isospin properties of the pion multiplets, the inelastic scattering of π^+ and π^- near the Δ_{33} resonance provides an independent method for determining these quantities [6–8]. In this energy region, the free π^+-p and π^--n amplitudes are $\sim$3 times larger than those of π^+-n and π^--p. Thus π^- scattering is more sensitive to the constituent neutrons, while π^+ scattering is more sensitive to the constituent protons. By taking advantage of this selectivity, one can extract the neutron-proton transition matrix elements from simultaneous fits of the π^- and π^+ scattering data. This provides new results for comparison with those extracted from (e,e') and (p,p') experiments [2].

In this work we present recent data on π^- and π^+ elastic and inelastic scattering for the low-lying states ($J=2$–8) in ^{208}Pb at 180 MeV. All of these data were obtained using the same apparatus and during the same period of time. Thus the experiment provides a very consistent set of data that can be used to determine the isoscalar/isovector characteristics of these states.

Our knowledge of the pion-nucleus interactions is somewhat limited compared to that of electromagnetic probes. To compare the results of different probes, the models used in the analysis of the pion data should be carefully examined. To explore the model dependence of the results obtained, distorted-wave impulse approximation (DWIA) calculations in both coordinate (r) [9,10] and momentum (p) [11–13] space were employed with the same geometry parameters for the ground-state and transition neutron and proton densities. Because of their strong interaction, the pions are sensitive primarily to densities in the surface region. Thus, in this first analysis, we have employed the simple vibrating density model ("collective form factors") for the inelastic transition densities. Both calculations can reproduce the experimental angular distributions well with appropriate deformation parameters. It is found that the ratios of neutron to proton multipole matrix elements obtained in the r- and p-space calculations are close to each other (within 3–5 %), while the differences of their magnitudes are about

---

*Also at Ben-Gurion University of the Negev, Beer-Sheva 84105, Israel.

†Present address: Lewis and Clark College, Portland, OR 97219.

‡Present address: MIT Bates Linear Accelerator Center, Middleton, MA 01949.

15–20%. Compared to the p-space calculations, the r-space absolute values for M_p are closer to the electromagnetic values; however, the ratios M_n/M_p agree well in both r and p space with those obtained earlier from (p,p')-(e,e') analysis for $T_p \geq 400$ MeV. The effects of varying the pion-nucleon interaction energy shift, the off-shell pion-nucleon interaction, and the form factors for the ground-state and transition densities in these calculations are discussed in Sec. IV.

II. EXPERIMENT

The experiment was performed using the Energetic Pion Channel and EPICS Spectrometer [14,15] at the Los Alamos Clinton P. Anderson Meson Physics Facility (LAMPF). The data were obtained using π^- and π^+ beams with an incident kinetic energy of $T_\pi = 180$ MeV, over the laboratory scattering angular range of $\theta_L \simeq 14°-60°$. An enriched ($>98\%$ pure) ^{208}Pb target with areal density $\simeq 100$ mg/cm^2 was used in the experiment. The overall energy resolution was <150 keV [full width at half maximum (FWHM)]. Ion chambers placed in the incident pion beam provided the relative normalization for the cross sections. The absolute normalization was obtained from comparison of the normalized yield for π^- and π^+ scattering from hydrogen measured during the experiment with the cross sections calculated using the program CROSS [16], which utilizes the phase shifts of Rowe, Salomon, and Landau [17].

The elastic and inelastic transition yields were extracted using the peak fitting code FIT [18], which used experimental line shapes. Typical excitation spectra for π^- and π^+ are shown in Figs. 1 and 2.

The data were corrected for the solid-angle variation across the spectrometer acceptance ($\simeq \pm 1.5°$) as well as for computer dead time, chamber efficiency, the number of pions decaying in flight, and the spectrometer momentum acceptance. The resulting overall uncertainty in the absolute cross-section normalization is estimated to be $\pm 8\%$.

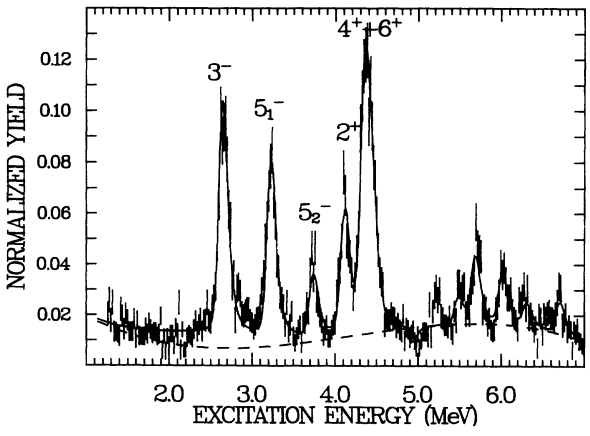

FIG. 1. Excitation spectrum of ^{208}Pb$(\pi^+,\pi^{+\prime})$ at $T_\pi = 180$ MeV, $\theta_{lab} = 29°$.

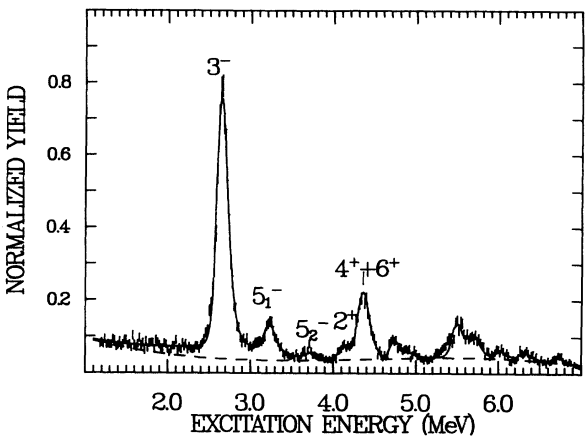

FIG. 2. Excitation spectrum of ^{208}Pb$(\pi^-,\pi^{-\prime})$ at $T_\pi = 180$ MeV, $\theta_{lab} = 14°$.

III. EXPERIMENTAL RESULTS AND ANALYSIS

A. Elastic scattering

The elastic differential cross sections measured during the experiment are shown in Fig. 3. Included in this figure are the results of DWIA calculations using the r-space code DWPI [9] and the p-space code PPT (a modified

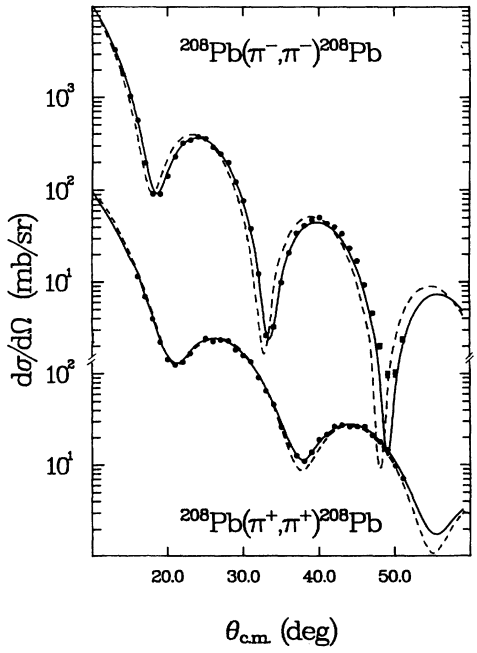

FIG. 3. Differential elastic cross sections for ^{208}Pb(π^-,π^-) and ^{208}Pb(π^+,π^+) at 180 MeV. The solid curves represent DWIA calculations in r space using 2PF densities (code DWPI) with energy shifts of 39 MeV (for π^+) and 30 MeV (for π^-). The dashed curves represent DWIA calculations in p space with the same density (code PPT), but with energy shifts of 25 MeV (for π^+) and 18 MeV (for π^-).

version of the code PIPIT [11]). A two-parameter Fermi (2 PF) distribution

$$\rho_i(r)=\rho_{0i}[1+\exp(r-R_i)/a_i]^{-1} \quad (1)$$

was used for the charge ($i=q$), neutron ($i=n$), and proton ($i=p$) ground-state densities. Our procedure was to calculate the values of R_p and a_p using $R_q=6.624$ fm, $a_q=0.549$ fm, and $\langle r_q^2\rangle^{1/2}=5.521$ fm for the charge density obtained from a 2PF fit to electron scattering and mu-mesic atom data [19]. The mean-square charge and proton radii are related by the unfolding relation

$$\langle r_p^2\rangle=\langle r_q^2\rangle-F_p^2 , \quad (2)$$

where F_p is the proton charge distribution rms radius inside the nucleus. In our calculation, F_p^2 was chosen to be $(1.0\text{ fm})^2$, based on a theoretical explanation of the European Muon Collaboration (EMC) effect [20]. An additional relation is needed to determine R_p and a_p uniquely. For a flat interior density such as the 2PF has, we can assume

$$\rho_{0q}=\rho_{0p} , \quad (3)$$

where ρ_{0i} ($i=p$, q, and n) are the normalized densities at the origin. The ρ_{0i} can be calculated with sufficient accuracy from the approximate volume integral of Eq. (1):

$$\rho_{0i}\simeq 3f_i/4\pi(R_i^3+\pi^2a_i^2R_i) , \quad (4)$$

where $f_i=Z$ when $i=q$ or p and $f_i=N$ for $i=n$. This gives $\rho_{0q}=\rho_{0p}=0.06308$ fm^{-3}. Using Eqs. (2)–(4), we then obtain $R_p=6.673$ fm, $a_p=0.448$ fm, and $\langle r_p^2\rangle^{1/2}=5.431$ fm. The R_n and a_n were then searched upon to fit the experimental elastic-scattering data. Because of the limited range of our elastic cross-section measurements ($\theta_L\simeq 14°$–$60°$), data from an earlier experiment at 162 MeV [21] which cover angles $\theta_L\simeq 10°$–$110°$ were also included in the search. The 2PF neutron parameters determined were $R_n=6.380$ fm and $a_n=0.610$ fm, giving $\langle r_n^2\rangle^{1/2}=5.437$ fm and $\rho_{0n}=0.1062$ fm^{-3}, which results in

$$\rho_0=\rho_{0n}+\rho_{0p}=0.169\text{ fm}^{-3} ,$$

a very reasonable value. The experimental data at 162 MeV and the fits with the r- and p-space calculations are shown in Figs. 4 and 5. The densities used here are compared with those from a Hartree-Fock-Bogoliubov (HFB) calculation [22] of the ^{208}Pb ground state and are shown in Fig. 6. The difference between the rms radii of the neutron and proton densities, Δr_{np} ($\equiv\langle r_n^2\rangle^{1/2}-\langle r_p^2\rangle^{1/2}$),

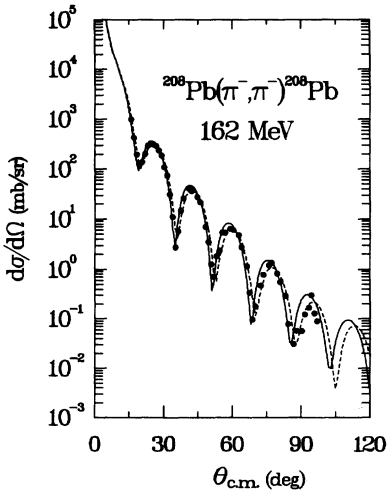

FIG. 4. Differential elastic cross sections for ^{208}Pb(π^-,π^-) at 162 MeV. The solid curve represents a DWIA calculation in p space (code PPT) with an energy shift of 12 MeV, and the dashed curve represents a DWIA calculation in r space with an energy shift of 23 MeV. The data are from Ref. [21]. The same 2PF densities were used as in Fig. 3.

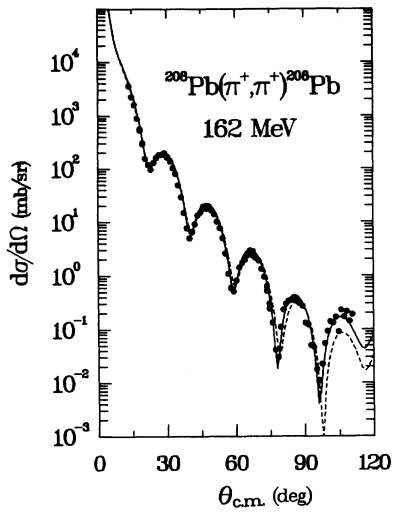

FIG. 5. Differential elastic cross sections for ^{208}Pb(π^+,π^+) at 162 MeV. The solid curve represents a DWIA calculation in p space (code PPT) with an energy shift of 19 MeV, and the dashed curve represents a DWIA calculation in r space with an energy shift of 32 MeV. The data are from Ref. [21]. The same 2PF densities were used as in Fig. 3.

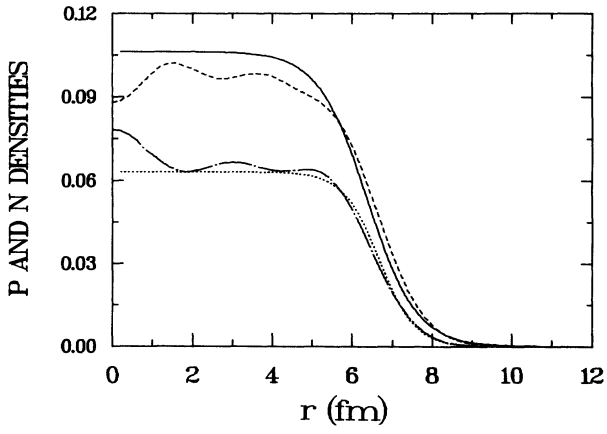

FIG. 6. Two-parameter Fermi distributions of neutron (ρ_n) and proton (ρ_p) used in the calculations and the corresponding HFB neutron (ρ_n^D), and proton (ρ_p^D) densities of Decharge and Gogny [22]. The solid, dotted, dashed, and dot-dashed curves represent the ρ_n, ρ_p, ρ_n^D, and ρ_p^D, respectively.

TABLE I. Energy shifts ΔE_r and ΔE_p of pion-nucleon center-of-mass energy used to evaluate the free pion-nucleon phase shifts.

Incident pion	Incident energy	ΔE_r	ΔE_p
π^-	162	23	12
π^+	162	32	19
π^-	180	30	18
π^+	180	39	25

can be calculated from the above parameters. It is found that, for a reasonable fit, Δr_{np} varies from 0 to 0.05 fm. This is somewhat smaller than the HFB value [22] ($\Delta r_{np}=0.13$ fm) and results from proton (and electron) scattering at $T_p=800$ MeV [23]. Other similar analyses [24,5] of pion scattering have found $\Delta r_{np}\simeq 0.02-0.06$ fm, which are also smaller than the HFB value. Because of the surface nature of pion-nucleus interaction, the fit is not very sensitive to the interior part of the densities used in the calculations. We will come back to this point again in Sec. IV C. Our smaller value of Δr_{np} may also indicate the need for medium modification of the pion-nuclear interaction.

Energy shifts for the pion-nucleon center-of-mass energy used in evaluating the free pion-nucleon phase shifts [21,25] were employed in both r- and p-space calculations. The values of the energy shifts for π^- and π^+ scattering at 162 and 180 MeV are listed in Table I. The difference between the energy shift in r and p space will be discussed in Sec. IV. The number of partial waves chosen in both r- and p-space calculations was taken to be 20 for good convergence of the nuclear scattering amplitude over the partial-wave sum. The matching radius $R_{\rm cut}$ in the PPT code was carefully searched for the best convergence of the calculated result with respect to its position and grid points [11].

B. Inelastic scattering

Collective-model [vibrating density model (VDM)] transition densities were used to analyze the inelastic-scattering data. The neutron and proton transition densities were assumed to have the form

$$\rho^i_{\rm tr}=-\beta_i R_i \frac{d\rho^i}{dr} , \tag{5}$$

where $i=p$ or n and the β_i's are the deformation parameters. In most of our calculations, the ρ^i's were chosen to be ground-state densities. The effects of the variation of ρ^i and $\rho^i_{\rm tr}$ will be discussed in Sec. IV.

The computer code DWPI [10] for the r-space calculations was modified to include higher angular momentum transfers, up to $J=8$. The code HL [12,13] for the p-space calculation was modified to have more Gaussian integration points, to allow higher angular momentum transfer, and to allow various options for using different neutron and proton densities. The normalization procedure in the collective macroscopic calculation of code HL was carefully checked and modified to get the correct

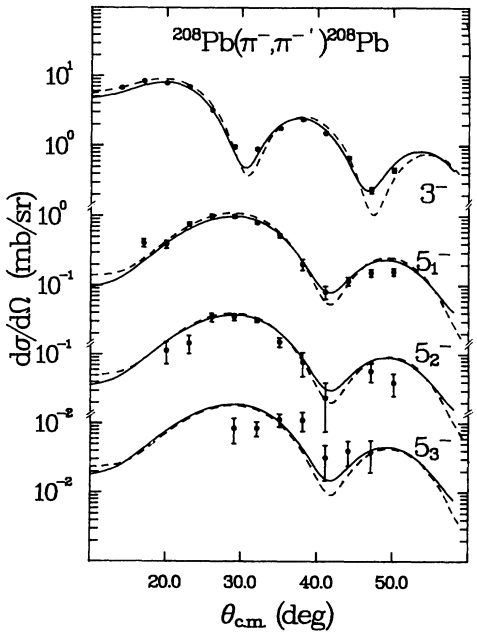

FIG. 7. Differential inelastic cross sections for ^{208}Pb($\pi^-,\pi^{-\prime}$) at 180 MeV for the 3^- (2.61 MeV), 5_1^- (3.20 MeV), 5_2^- (3.71 MeV), and 5_3^- (3.96 MeV) states. The solid curves represent DWIA calculations in r space (code DWPI) at an energy shift of 30 MeV, and the dashed curves represent DWIA calculations in p space (code HL) at an energy shift of 18 MeV.

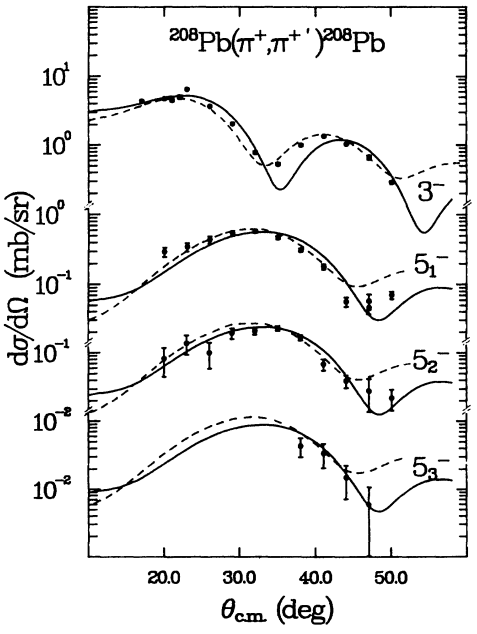

FIG. 8. Differential inelastic cross sections for ^{208}Pb($\pi^+,\pi^{+\prime}$) at 180 MeV for the 3^- (2.61 MeV), 5_1^- (3.20 MeV), 5_2^- (3.71 MeV), and 5_3^- (3.96 MeV) states. The solid curves represent DWIA calculations in r space (code DWPI) at an energy shift of 39 MeV, and the dashed curves represent DWIA calculations in p space (code HL) at an energy shift of 25 MeV.

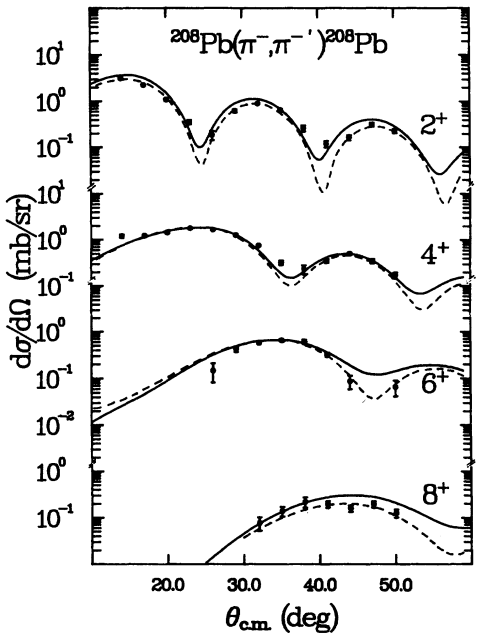

FIG. 9. Differential inelastic cross sections for ^{208}Pb (π^-, $\pi^{-\prime}$) at 180 MeV for the 2^+ (4.09 MeV), 4^+ (4.32 MeV), 6^+ (4.42 MeV), and 8^+ (4.61 MeV) states. The solid curves represent DWIA calculations in r space (code DWPI) at an energy shift of 30 MeV, and the dashed curves represent DWIA calculations in p space (code HL) at an energy shift of 18 MeV.

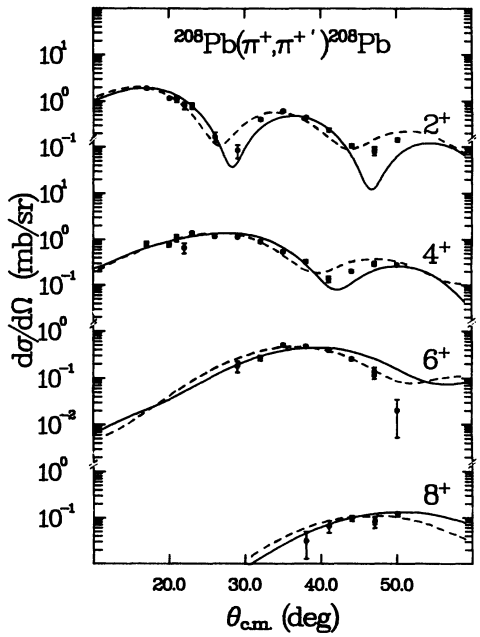

FIG. 10. Differential inelastic cross sections for ^{208}Pb(π^+,$\pi^{+\prime}$) at 180 MeV for the 2^+ (4.09 MeV), 4^+ (4.32 MeV), 6^+ (4.42 MeV), and 8^+ (4.61 MeV) states. The solid curves represent DWIA calculations in r space (code DWPI)at an energy shift of 39 MeV, and the dashed curves represent DWIA calculations in p space (code HL) at an energy shift of 25 MeV.

β_p and β_n as defined in Eq. (5).

The experimental data for the inelastic angular distributions, the fits using the modified r-space code DWPI, and the fits using the p-space code HL are presented in Figs. 7–10. The neutron and proton deformation parameters β_n and β_p, respectively, were adjusted in both calculations to produce the best fits for the π^- and π^+ cross sections simultaneously. In order to compare the results obtained from these two calculations, the theoretical curves were fitted to the same pair of experimental points for each excited state in π^- and π^+ scattering, thus yielding a unique pair (β_n,β_p) in each space. In most cases the points were chosen around the first maximum for the π^- and π^+ cross sections. We estimate that the uncertainties of the β_i's determined by this method are 3.5–6% as a result of the errors in the measured differential cross sections and the choices of the experimental data points. The errors are somewhat larger for the weakly excited 5_3^- state.

Coulomb excitation effects at 180 MeV have been

TABLE II. Neutron and proton deformation parameters, transition matrix elements, and $\hat{M}_n/\hat{M}_p$ ratios calculated in r space for low-lying states in ^{208}Pb.

		This experiment					EM[a]
E_{ex} (MeV)	J^π	β_n[b]	β_p[b]	M_n[c]	M_p[c]	$\hat{M}_n/\hat{M}_p$	M_p
2.63	3^-	0.149	0.122	1.40×10^3	7.78×10^2	1.17	$7.88(10)\times10^2$
3.20	5_1^-	0.081	0.062	4.13×10^4	2.04×10^4	1.31	$2.11(7)\times10^4$
3.71	5_2^-	0.049	0.042	2.47×10^4	1.41×10^4	1.14	$1.55(6)\times10^4$
3.96	5_3^-	0.037	0.022	1.88×10^4	7.35×10^3	1.66	2.83×10^3
4.09	2^+	0.069	0.052	9.13×10^1	4.75×10^1	1.25	$5.64(14)\times10^1$
4.32	4^+	0.087	0.078	5.91×10^3	3.56×10^3	1.08	$3.94(13)\times10^3$
4.42	6^+	0.075	0.072	2.93×10^5	1.77×10^5	1.08	$2.58(13)\times10^5$
4.61	8^+	0.064	0.049	1.58×10^7	6.80×10^6	1.52	$7.35(61)\times10^6$

[a]Electromagnetic value from Ref. [1] where the experimental references are given. Errors in the last digits are given in parentheses.

[b]$R_n=6.380$ fm, $R_p=6.673$ fm.

[c]Units for M_n are fm$^\lambda$, and for M_p, e fm$^\lambda$.

TABLE III. Neutron and proton deformation parameters, transition matrix elements, and $\hat{M}_n/\hat{M}_p$ ratios calculated in p space for low-lying states in ^{208}Pb.

		This experiment					EM[a]
E_{ex} (MeV)	J^π	β_n [b]	β_p [b]	M_n [c]	M_p [c]	$\hat{M}_n/\hat{M}_p$	M_p
2.63	3^-	0.127	0.106	1.19×10^3	6.80×10^2	1.14	$7.88(10)\times10^2$
3.20	5_1^-	0.067	0.051	3.41×10^4	1.68×10^4	1.32	$2.11(7)\times10^4$
3.71	5_2^-	0.040	0.037	2.05×10^4	1.23×10^4	1.15	$1.55(6)\times10^4$
3.96	5_3^-	0.031	0.021	1.55×10^4	6.83×10^3	1.48	2.83×10^3
4.09	2^+	0.056	0.043	7.45×10^1	3.89×10^1	1.25	$5.64(14)\times10^1$
4.32	4^+	0.071	0.061	4.80×10^3	2.81×10^3	1.11	$3.94(13)\times10^3$
4.42	6^+	0.066	0.063	2.57×10^5	1.54×10^5	1.08	$2.58(13)\times10^5$
4.61	8^+	0.058	0.044	1.45×10^7	6.01×10^6	1.56	$7.35(61)\times10^6$

[a]Electromagnetic value from Ref. [1] where the experimental references are given. Errors in the last digits are given in parentheses.
[b]$R_n=6.380$ fm, $R_p=6.673$ fm.
[c]Units for M_n are fm$^\lambda$, and for M_p, $e$fm$^\lambda$.

shown to be small [26] and hence were not included in our analysis.

The agreement between the calculated cross sections and data is quite good for all the states analyzed except the weak 5_3^- state. From electron scattering [27] and a theoretical Hartree-Fock random-phase-approximation (HF-RPA) calculation [28], it has been shown that the 5_3^- state has a quite different transition density from the simple collective-model macroscopic form. We will come back to this problem again in Sec. IV.

The sensitivity of the deformation parameters to the absolute cross-section normalization was investigated by varying the experimental cross sections by $\pm8\%$. The resulting deformation parameters were found to vary by ~2–4%.

The neutron and proton multipole matrix elements $[M_i(\lambda),\ i=n \text{ or } p]$ are related to the transition densities by

$$M_i(\lambda)\equiv\int_0^\infty \rho_{tr}^i(r)r^{\lambda+2}dr \ . \tag{6}$$

For the two-parameter Fermi distribution, many authors use the approximate relation

TABLE IV. Reduced neutron-proton transition matrix element ratios $\hat{M}_n/\hat{M}_p$, for ^{208}Pb obtained from this and other analyses.

Probe	T_{inc} (MeV)	3^-	5_1^-	5_2^-	5_3^-	2^+	4^+	6^+	8^+	Analysis method[a]	References
π^-/π^+	180	1.17	1.31	1.14	1.66	1.25	1.08	1.08	1.52	VDM	this work[b]
π^-/π^+	180	1.14	1.32	1.15	1.48	1.25	1.11	1.08	1.56	VDM	this work[c]
π^-/π^+	116	1.03								VDM	26[d]
π^-/π^+	120	1.20				1.07	0.94			VDM	26[d,e]
π^-/π^+	180	1.19				1.05				VDM	26[d,f]
π^-/π^+	250	1.09				1.04	0.87			VDM	26[d]
π^-/π^+	291	1.03								VDM	26[d,g]
p/e	h	1.13 (5)	1.23 (7)	1.11 (3)		1.30 (4)	1.13 (4)	0.93 (14)	1.60 (20)	various	2[h]
p/e	i	0.97 (11)	0.97 (13)	0.82 (8)		0.95 (9)	0.92 (9)	0.70 (15)	1.12 (15)	various	2[i]
α/e	104	1.19								MI	32
Theory		1.06								*P.* − *Vib.* coupling	33
Theory		1.00	1.23	0.69		0.93	0.91	0.85		RPA	28

[a]VDM, vibrating density model, $\rho_{tr}=-\beta R\partial\rho_0/\partial r$; VPM, vibrating potential model, $V_{tr}=-\beta R\partial U_{opt}/\partial r$; MI, model-independent analysis.
[b]Results obtained in r-space calculation. Coulomb excitation was not included.
[c]Results obtianed in p-space calculation. Coulomb excitation was not included.
[d]Coulomb excitation was included.
[e]Reanalysis of Ref. [30] data by Ref. [26].
[f]Reanalysis of this data by Ref. [26].
[g]Reanalysis of Ref. [31] data by Ref. [26].
[h]Average of values from $T_p=500$ and 800 MeV by various methods. See Ref. [2]. Errors in last digits are given in parentheses.
[i]Average of values from $T_p=35$–400 MeV by various methods. See Ref. [2]. Errors in last digits are given in parentheses.

$$M_i(\lambda)\simeq 3P_i\beta_i R_i^{\lambda}\{1+[(\lambda+4)(\lambda-1)/6]\pi^2 a_i^2/R_i^2\}/4\pi\ , \tag{7}$$

where $P_i=Z$ when $i=p$ and $P_i=N$ when $i=n$. When $(a/R)\sim 0.1$, the error due to this approximation is less than 2% for $\lambda\leq 4$, but becomes larger when $\lambda>4$. All values of M_i listed in our tables were calculated from Eq. (6) rather than Eq. (7). The reduced multipole matrix elements are given by $\hat{M}_i(\lambda)=M_i(\lambda)/P_i$. Therefore, the reduced multipole-matrix-element ratios were calculated from

$$\hat{M}_n/\hat{M}_p=(Z/N)M_n/M_p\ . \tag{8}$$

The neutron and proton deformation parameters for the excited states, their corresponding multipole matrix elements, and the ratios of the reduced matrix elements from the r- and p-space calculations are listed in Tables II and III, respectively. The reduced transition probabilities are given by

$$\begin{aligned} B(i,\lambda)&=|P_i\hat{M}_i(\lambda)|^2 \\ &=|M_i(\lambda)|^2 \\ &=[P_i(\lambda+2)\beta_i R_i\langle r^{\lambda-1}\rangle_i/4\pi]^2\ . \end{aligned} \tag{9}$$

Our values of M_p can be compared with M_q obtained by electromagnetic methods [see Eq. (6)], since, by Satchler's theorem [29], the charge and proton moments should be equal (ignoring the neutron charge form factor). The best available (or weighted average) of the electromagnetic amplitudes M_q ($\simeq M_p$) are given in Tables II and III. Table IV lists the ratios $\hat{M}_n/\hat{M}_p$ obtained in this work along with previous results from different probes at different energies [26,30–32] employing various analysis methods. For comparison, theoretical predictions [28,33] are also included in Table IV.

It can be seen that the reduced multipole-matrix-elements ratios of the r-space calculations are very close to those of the p-space calculations, as well as to those from other probes, except for the $J=6$ and 8 states. This indicates that the ratios are less model dependent than the matrix elements themselves. On the average, the matrix elements obtained from p-space calculations are smaller than those in r space by 15–20 %. Because of the difference in equations of motion, pion-nucleon interactions, and methods of dealing with the Coulomb interaction and other approximations that are used in these two calculations, it is not clear to us which factor is more important. Some possibilities are discussed in Sec. IV. With such a simple collective macroscopic model, it is remarkable that the multipole matrix elements and corresponding transition probabilities obtained from the analysis of pion-scattering data are close to those derived from the electromagnetic measurements, as reported previously [8]. It is well known that some important factors such as the Δ dynamics [34–38] and higher-order effects in Kerman-McManus-Thaler theory [39] are missing in these codes. More work to study these effects is very desirable.

IV. DISCUSSION

To explore the model dependence of the results obtained, the effects of changing some dynamical and geometric parameters were investigated. We will concentrate our attention on the well-established states such as the 2_1^+ and 3_1^- and perform the test calculations in p space. The 2_1^+ state is only moderately collective [$B(E2)\simeq 10$ Weisskopf units], but all of the low-lying states analyzed here (except for the 5_3^-) have surface-peaked charge transition densities [27] which are quite close in shape to the VDM densities we have used. Therefore, similar results are expected for the other states as well as for the r-space calculations.

A. Energy shifts in the pion-nucleon interaction

It has been customary to take the energy shifts used in evaluating the pion-nucleon interaction as empirical parameters in fitting the pion-nucleus scattering data [21,25]. It has been argued that this shift is mainly due to the Coulomb repulsion (or attraction, depending on the charge of the incident pion) and nuclear binding effects [21,40,41]. The effect of including an energy shift is mainly to alter the depths of the minima rather than to shift their angular positions. In the modified r-space DWPI code, the coefficients of the standard Kisslinger potential are determined by πN phase shifts at a shifted center-of-mass pion-nucleon energy $E_r=E_{\text{c.m.}}-\Delta E_r$, and in the p-space PPT code, the on-shell πN t-matrix elements are obtained from the πN phase shifts at an energy $E_p=E_{\text{c.m.}}-\Delta E_p$. The use of different energy shifts in r and p space means that the free pion-nucleon interactions chosen in these two spaces are at slightly different energies. It is well known that the free pion-nucleon interac-

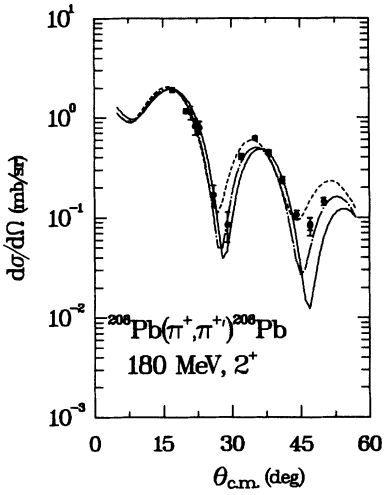

FIG. 11. Differential inelastic cross sections for ^{208}Pb($\pi^+,\pi^{+\prime}$) at 180 MeV for 2^+ (4.09 MeV) state. The solid curve represents a DWIA calculation in r space (code DWPI) at an energy shift of 39 MeV. The dashed curve represents a DWIA calculation in p space (code HL) at an energy shift of 25 MeV. The dot-dashed curve represents a DWIA calculation in p space (code HL) at an energy shift of 39 MeV. In the last two calculations, the β_i's are the same.

tion shows a strong energy dependence. So it is expected that the difference between ΔE_r and ΔE_p would have an important effect on the results obtained. To check this a p-space calculation for the 2^+ state was performed using ΔE_r instead of ΔE_p. The result is shown in Fig. 11. It can be seen that the result is close to that from the r-space calculation. The differences between the phenomenological ΔE_i for π^- and π^+ may be due to the different sign of the pion-nucleus Coulomb interaction, but the magnitudes of the differences found are smaller than that estimated [21,40]. It seems to us that a more clear physical understanding of these energy shifts in the two spaces is needed.

B. Off-shell models in the pion-nucleon interaction

The Landau-Tabakin (LT) off-shell model [42] of the pion-nucleon t matrix is used in the p-space code PPT. At high-momentum transfer (q), the Kisslinger potential which is used in the r-space calculation is divergent, while in the LT model of the off-shell matrix elements are designed to converge to zero at high q. For scattering at large angles, it seems that the LT model is physically more reasonable.

The fall off or damping factors α_l's in the LT model are chosen to be close to those obtained from Regge-pole theory [42]. In order to compare with the results from the r-space calculation, a calculation in p space was performed using values of the α_l's reduced by a factor of 10. A reduction of α_l will decrease the rate of falloff as q increases. With this modification of α_l, it is found that the matrix element M_p of the 2^+ state increases by $\sim 5\%$ relative to its original value in the p-space calculation, while it increases $\sim 3\%$ for the 3^- state.

At low pion incident energy, below the Δ-resonance region, the nucleus is more transparent to pions and there the difference between the off-shell models is expected to have a more important effect. The elastic and inelastic

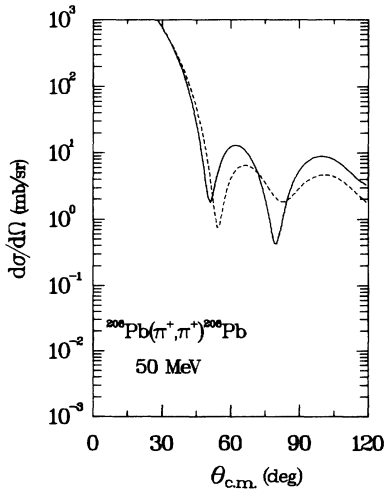

FIG. 12. Differential elastic cross sections for ^{208}Pb(π^-,π^-) at 50 MeV. The solid curve represents a DWIA calculation in p space (code PPT), and the dashed curve represents a DWIA calculation in r space (code DWPI) both without energy shifts.

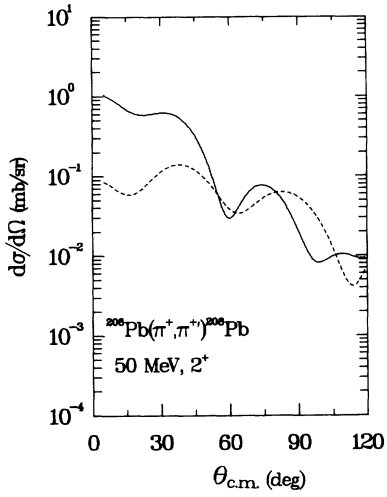

FIG. 13. Differential inelastic cross sections for ^{208}Pb(π^+,$\pi^{+\prime}$) at 50 MeV for the 2^+ (4.09 MeV) state. The dashed curve represents a DWIA calculation in r-space (code DWPI). The solid curve represents a DWIA calculation in p space (code HL).

scatterings to the 2^+ state were calculated at 50 MeV with the same β_i's and ΔE's (set to zero) in both r and p space. The comparisons are shown in Figs. 12 and 13. It can be seen that the differences between the results from these two calculations are bigger than at 180 MeV. At high pion incident energy, above the Δ-resonance region, the nucleus is also more transparent, and more pion-nucleus and pion-nucleon partial waves are involved. Thus a more realistic off-shell model is also important at higher energies. A more careful study of off-shell effects and a search for better representations of the interaction are desirable.

C. Changes in the ground-state density

The effect of varying the 2PF geometry parameters of the ground-state density and the use of microscopic point densities were also investigated. In agreement with the theoretical HFB calculation [22], the central proton density ρ_{0p} is slightly larger than ρ_{0q}. Choosing $\rho_{0p}=1.045\rho_{0q}$, we get $R_p=6.538$ fm and $a_p=0.531$ fm from Eqs. (2)–(4). With these parameters and keeping R_n and a_n fixed, the p-space calculation can reproduce the elastic data well with an energy shift of 24.0 MeV for π^+. Using the resulting optical potential as new input for the HL code, it was found that the M_p of the 2^+ state is increased by $\sim 3\%$. A less model-dependent method is to calculate the proton density $\rho_p(r)$ by unfolding the proton charge form factor from the charge density obtained from electron scattering. The neutron density is then computed from the equation

$$\rho_n=(N/Z)\rho_p+s(\rho_n^D-(N/Z)\rho_p^D)\ , \tag{10}$$

where $\rho_{n(p)}^D$ denotes the HFB neutron (proton) density of Decharge and Gogny [22] and s is the sign of $(\rho_p\rho_p^D)$ at $|\rho_p|_{\max}$. If the charge distribution inside the proton has

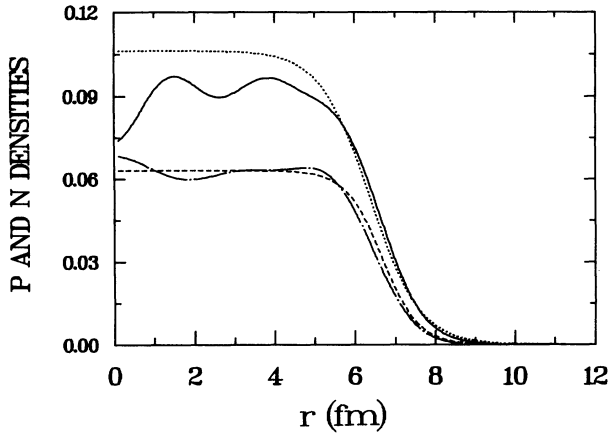

FIG. 14. Unfolded proton and neutron densities and the two-parameter Fermi proton and neutron densities. The dot-dashed curve represents the unfolded proton density calculated from the (e,e') charge density, and the solid curve represents the neutron density from Eq. (10). The dashed and dotted curves represent the 2PF proton and neutron densities, respectively.

the form $f_p(\mathbf{r})=N\exp(-\alpha r)$, where N is the normalization constant and α is determined from the proton rms radius (1.0 fm), then the unfolded proton density $\rho_p(r)$ and the neutron density $\rho_n(r)$ obtained from Eq. (10) are as shown in Fig. 14. With these densities the DWIA calculations of the elastic scattering in p space using code PPT were performed. The results along with those obtained using the two-parameter Fermi distribution are compared with experimental data in Fig. 15. It can be seen that, although the interior parts of the unfolded proton and neutron densities obtained from Eq. (10) are quite different from that of the two-parameter Fermi distribution, the two fits of the elastic scattering are very similar. This is again due to the surface nature of the interaction near the resonance region. Of course, the difference in the interior parts of the proton and neutron densities has an effect on some physical quantities. For example, the difference between the rms radii, Δr_{np}, of the unfolded proton and neutron densities obtained from Eq. (10) is 0.13 fm, which is larger than our previous result (see Sec. III A), but close to that obtained from other experiments and the HFB value [22]. The DWIA calculation of the elastic scattering generates distorted waves that are somewhat different from the two-parameter Fermi distribution. With these new distorted waves and the collective 2PF transition densities, the DWIA calculations of the inelastic scattering in p space were performed using code HL. The results and a comparison with experimental data and previous results (see Sec. III B) for the 3^- state are shown in Fig. 16. It can be seen that the two results are quite close with only a slight difference in the β_i's ($\sim$3–6 %).

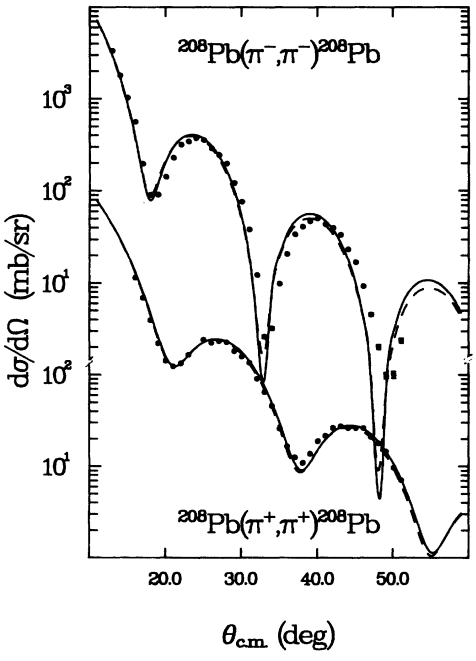

FIG. 15. Differential elastic cross sections for ^{208}Pb(π^-,π^-) and ^{208}Pb(π^+,π^+) at 180 MeV. The solid curves represent the DWIA calculations in p space (code PPT) at energy shifts of 25 MeV (for π^+) and 18 MeV (for π^-) and using the unfolded proton and neutron densities. The dashed curves represent the DWIA calculations in p space (code PPT) with 2PF proton and neutron densities at the same energy shifts as above.

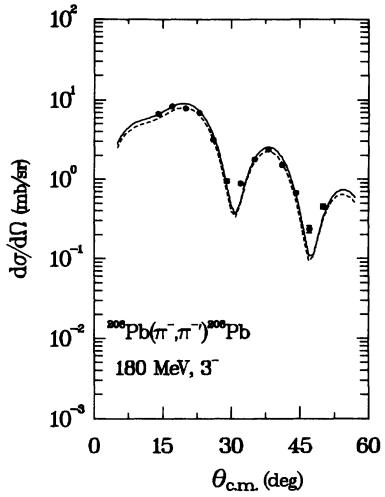

FIG. 16. Differential inelastic cross sections for ^{208}Pb($\pi^-,\pi^-{}'$) at 180 MeV for the 3^- (2.61 MeV) state. The dashed curve represents a DWIA calculation in p space (code HL) at an energy shift of 25 MeV and using the unfolded proton and neutron ground-state densities and VDM transition densities from the 2PF distributions. The solid curve represents a DWIA calculation in p space (code HL) with 2PF proton and neutron ground-state densities at the same energy shift as above and VDM transition densities from the 2 PF distributions.

D. Effect of the transition form factor

The transition form factor $\rho^i_{\rm tr}=-\beta_i R_i d\rho^i(r)/dr$ is characterized by the width and location of its peak. These quantities are directly connected to the diffuseness

a and the half-value radius R in the two-parameter Fermi distribution. In the simple VDM, the $\rho^i(r)$'s are usually taken to be the ground-state densities. We explored the effect of changing the transition form factor by varying a_i and R_i in ρ^i. We chose $a_i'=\frac{2}{3}a_i$ and $R_i'=R_i\pm0.5$ fm, and repeated the calculations for the 2^+ states, keeping the ground-state densities unchanged. The results are shown in Figs. 17 and 18. In the region of the data ($\theta_L=14°-60°$), the effects of variations in R and a are small when the β's are rematched, but at larger angles the effects are more noticeable. As expected, for the smaller half-value radius, the first diffractive minimum is shifted to a larger angle. The calculations follow the same trend for the smaller diffuseness.

If the ground-state and transition densities are changed simultaneously, the resulting shift of the first diffraction minimum is larger. This result for $a_i'=\frac{2}{3}a_i$ is also shown in Fig. 17. Similar shifts of the diffractive minima in the elastic-scattering cross section are also observed. This indicates the close relation between the elastic scattering and inelastic reaction, especially near the resonance energy (strong absorption region) [43].

As indicated by the (e,e') scattering [27] and the HF-RPA calculation [28], the transition density for certain states is quite different from that given by the simple macroscopic collective model. A typical example is the third 5^- state in ^{208}Pb. The first peak of the charge transition density is near 4.0 fm and is stronger than the second peak (near 7.0 fm). Some calculations [27] also suggest that the second maximum might in fact be a minimum. Some trial proton and neutron transition densities ρ_p^{tr} and ρ_n^{tr} designed to simulate the forms suggested

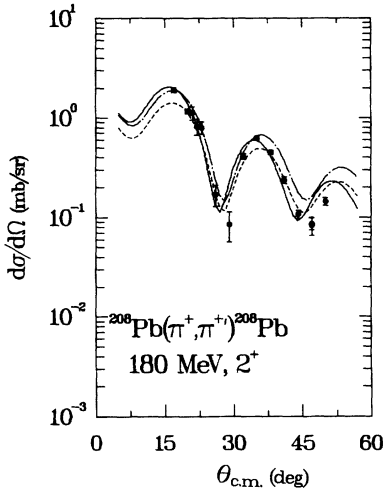

FIG. 17. Differential inelastic cross sections for ^{208}Pb$(\pi^+,\pi^{+\prime})$ at 180 MeV for the 2^+ (4.09 MeV) state. The solid curve represents a DWIA calculation in p space with diffuseness $a_p=0.448$ fm and $a_n=0.610$ fm. The dashed curve represents a DWIA calculation in p space with diffuseness $a_i'=\frac{2}{3}a_i$ in code HL (inelastic). The dot-dashed curve represents a DWIA calculation in p space with diffuseness $a_i'=\frac{2}{3}a_i$ in both the codes PPT (elastic) and HL (inelastic). All calculations were performed with fixed R_i's and β_i's.

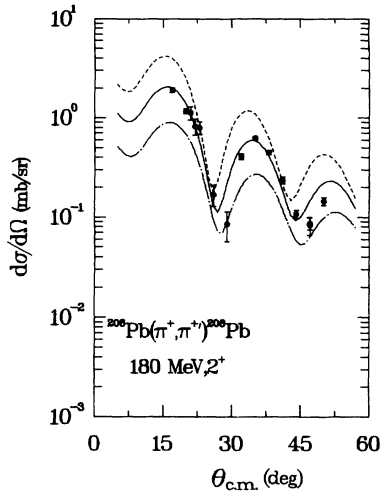

FIG. 18. Differential inelastic cross sections for ^{208}Pb$(\pi^+,\pi^{+\prime})$ at 180 MeV for 2^+ (4.09 MeV) state. The solid curve represents a DWIA calculation in p space with half-value radii of $R_p=6.673$ fm and $R_n=6.380$ fm. The dashed curve represents a DWIA calculation in p space with half-value radii of $R_i'=R_i+0.5$ fm in code HL (inelastic). The dot-dashed curve represents a DWIA calculation in p space with half-value radii of $R_i'=R_i-0.5$ in code HL (inelastic). All calculations were performed with fixed a_i's and β_i's.

are shown in Fig. 19. Three combinations of these densities were employed in our calculation for the 5_3^- state: (a) the second maximum in both ρ_p^{tr} and ρ_n^{tr} was kept fixed, (b) the second maximum in ρ_n^{tr} was changed to a minimum, while that in ρ_p^{tr} was kept fixed, and (c) the second maximum in both ρ_p^{tr} and ρ_n^{tr} was changed to a minimum. The results are shown in Fig. 20. Comparing these results with those from the simple collective model, it is clear that because of the strong absorption, π-nucleus scattering near the Δ resonance is not very sensitive to the interior region of the transition density.

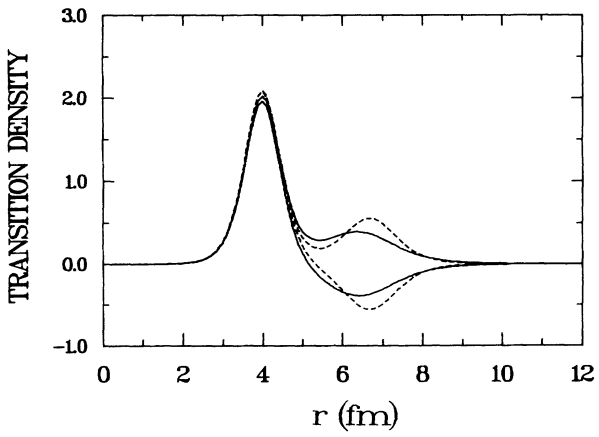

FIG. 19. Trial neutron and proton transition densities for the 5_3^- state in ^{208}Pb used in the calculations shown in Fig. 20. The solid and dashed curves represent the neutron and proton densities, respectively.

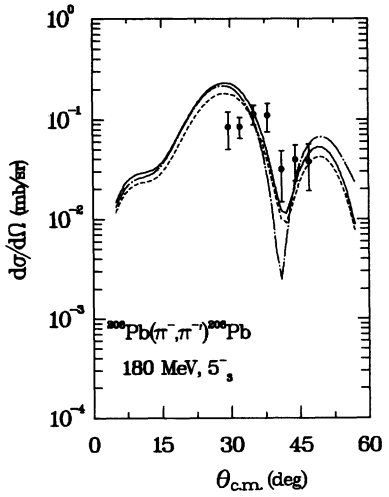

FIG. 20. Differential inelastic cross sections for ^{208}Pb($\pi^+,\pi^{+\prime}$) at 180 MeV for the 5^-_3 (3.96 MeV) state calculated in p space with various combinations of trial transition densities shown in Fig. 19. The solid curve represents a DWIA calculation for which the second maximum in both ρ_p^{tr} and ρ_n^{tr} is kept fixed. The dashed curve represents the case when the second maximum in only ρ_p^{tr} is changed to a minimum, whereas the dot-dashed curve shows the effect of changing the second maximum in both ρ_p^{tr} and ρ_n^{tr} to a minimum.

V. SUMMARY AND CONCLUSIONS

DWIA calculations were performed in both coordinate (r) and momentum (p) space for new data on π^+ and π^- scattering from ^{208}Pb at $T_\pi = 180$ MeV. For elastic scattering the 2PF proton density was derived from charge densities obtained from electron scattering. The neutron density and pion energy shifts were adjusted to get the best overall fits to the elastic π^+ and π^- data from this experiment and an earlier experiment [21] at 162 MeV. The fits are comparable in the r- and p-space calculations, but the neutron density used gives a value of $\Delta r_{np} \simeq 0$ (neutron-proton rms radii difference) in disagreement with theory and proton-scattering results ($\Delta r_{np} \simeq 0.1-0.2$).

For inelastic scattering the distorted waves used were those generated in the elastic-scattering calculation. The inelastic transition densities were taken as proportional to the derivative of the ground-state densities used for elastic scattering ("collective form factors" or vibrating density model). This simple model represents the data quite well in both r- and p-space calculations. The ratios of the transition matrix elements, M_n/M_p, calculated from the deformation parameters, are in good agreement with each other (r and p space) and with those obtained independently by a comparison of proton (or alpha) and electron scattering. In addition, the absolute values of the M_p from the r-space calculation are fairly close to those from electromagnetic methods, except for the non-collective 5^-_3 state, and the two high-spin states for which the collective form factors are expected to be inadequate. However, the M_p's from the p-space calculations are $\simeq 15-20\,\%$ lower than the electromagnetic values.

The inelastic angular distributions show only slight sensitivity to variations in the width and centroid of the transition density, indicating that pion scattering near the Δ resonance is mainly sensitive to an integral property of the density, such as the transition matrix elements. Calculations comparing different transition densities such as a VDM from the 2PF distributions, an unfolded distribution [Eq. (10)], and the densities of Decharge and Gogny show that the differences between transition matrix elements obtained are $\sim 15-20\,\%$.

Elastic-scattering calculations using a proton density from electron scattering and a neutron density from Eq. (10) give results quite close to those obtained using the 2PF densities. Both show a small shift in phase (to smaller θ for π^- and larger θ for π^+) relative to the data at 180 MeV. It is not clear whether this effect can be explained by medium modifications of the pion-nucleon interaction as is the case for proton- and kaon-nucleus scattering [44,45] or by Δ-dynamics effects.

In conclusion, it appears that pion scattering near the 33 resonance can give reliable neutron and proton transition matrix elements for transitions with surface peaked densities, but is not sensitive to the detailed shape of the transition density, especially in the interior region ($r \leq R_{1/2}$). Further, presently available reaction models are not good enough to give accurate determinations of ground-state neutron and proton densities, even in the surface region.

ACKNOWLEDGMENTS

We are grateful to M. Bryan, P. B. C. Dale, A. Fuentes, J. Garza, M. Machuco, M. Plum, P. Seidl, M. Smithson, and A. Williams for assistance in taking data. We are also indebted to T. -S. H. Lee for many helpful discussions. Special thanks are given to A. Sethi for his help in preparing the manuscript. This work was supported in part by grants from the U.S. Department of Energy and the Minnesota Supercomputer Institute.

[1] M. M. Gazzaly, N. M. Hintz, G. S. Kyle, R. K. Owen, G. W. Hoffmann, M. Barlett, and G. Blanpied, Phys. Rev. C **25**, 408 (1982).

[2] N. M. Hintz, D. Cook, M. Gazzaly, M. A. Franey, M. L. Barlett, G. W. Hoffmann, R. Fergerson, J. McGill, G. Pauletta, R. L. Boudrie, J. B. McClelland, and K. W. Jones, Phys. Rev. C **37**, 692 (1988), and references therein.

[3] S. J. Seestrom-Morris, D. Dehnhard, M. A. Franey, D. B. Holtkamp, C. L. Blilie, C. L. Morris, J. D. Zumbro, and H. T. Fortune, Phys. Rev. C **37**, 2057 (1988).

[4] S. Mordechai, C. Harvey, W. B. Cottingame, P. A. Seidl, C. F. Moore, L. C. Bland, M. Carchidi, H. T. Fortune, S. J. Seestrom-Morris, and C. L. Morris, Phys. Rev. C **36**, 1950 (1987).

[5] D. S. Oakley, M. J. Smithson, S. Mordechai, C. F. Moore, P. A. Seidl, C. L. Morris, G. C. Idzorek, Z. F. Wang, R. Gilman, J. D. Zumbro, H. T. Fortune, S. J. Seestrom-Morris, K. S. Dhuga, and D. L. Watson, Phys. Rev. C **35**,

1392 (1987).
[6] C. L. Morris, Phys. Rev. C **13**, 1755 (1976).
[7] D. B. Holtkamp, S. J. Seestrom-Morris, D. Dehnhard, H. W. Baer, C. L. Morris, S. J. Greene, C. J. Harvey, D. Kurath, and J. A. Carr, Phys. Rev. C **31**, 957 (1985).
[8] C. L. Morris, S. J. Seestrom-Morris, D. Dehnhard, C. L. Blilie, R. Gilman, G. P. Gilfoyle, J. D. Zumbro, M. G. Burlein, S. Mordechai, H. T. Fortune, L. C. Bland, M. Brown, D. P. Saunders, P. A. Seidl, C. Fred Moore, K. Maeda, G. S. Blanpied, and B. A. Brown, Phys. Rev. C **35**, 1388 (1987).
[9] R. A. Eisenstein and G. A. Miller, Comput. Phys. Commun. **8**, 130 (1974).
[10] R. A. Eisenstein and G. A. Miller, Comput. Phys. Commun. **11**, 95 (1976).
[11] R. A. Eisenstein and F. Tabakin, Comput. Phys. Commun. **12**, 237 (1976).
[12] T. -S. H. Lee and F. Tabakin, Nucl. Phys. **A226**, 253 (1974).
[13] T. -S. H. Lee and D. Kurath, Phys. Rev. C **21**, 293 (1980).
[14] H. A. Thiessen and S. Sobttka, Los Alamos National Laboratory Report No. LA-4534MS, 1970 (unpublished).
[15] T. G. Masterson, J. J. Kraushaar, R. J. Peterson, R. S. Raymond, R. A. Ristinen, R. L. Boudrie, E. F. Gibson, and A. W. Thomas, Phys. Rev. C **26**, 2091 (1982).
[16] G. R. Burleson and J. F. Amann, computer program CROSS (unpublished).
[17] G. Rowe, M. Salomon, and R. H. Landau, Phys. Rev. C **18**, 584 (1978).
[18] C. L. Morris, computer program FIT (unpublished).
[19] C. W. de Jager, H. de Vries, and C. deVries, At. Data Nucl. Data Tables **14**, 479 (1974).
[20] F. E. Close, R. G. Roberts, and G. G. Ross, Phys. Lett. **129B**, 346 (1983); R. L. Jaffe, F. E. Close, R. G. Roberts, and G. G. Ross, *ibid.* **134B**, 449 (1984).
[21] C. Olmer, D. F. Geesaman, B. Zeidman, S. Chakravarti, T. -S. H. Lee, R. L. Boudrie, R. H. Siemssen, J. F. Amann, C. L. Morris, H. A. Thiessen, G. R. Burleson, M. J. Devereux, R. E. Segel, and L. W. Swenson, Phys. Rev. C **21**, 254 (1980).
[22] J. Decharge and D. Gogny, Phys. Rev. C **21**, 1568 (1980); Centre d'Etudes de Bruyéres-le-châtel Report No. CEA-N-2260, 1982 (unpublished).
[23] G. W. Hoffmann, L. Ray, M. Barlett, J. McGill, G. S. Adams, G. J. Igo, F. Irom, A. T. M. Wang, C. Whitten, Jr., R. L. Boudrie, J. F. Amann, C. Glashausser, N. M. Hintz, G. S. Kyle, and G. S. Blanpied, Phys. Rev. C **21**, 1488 (1980).
[24] K. G. Boyer, W. B. Cottingame, L. E. Smith, S. J. Greene, C. Fred Moore, J. S. McCarthy, R. C. Minehart, J. F. Davis, G. R. Burleson, G. Blanpied, C. A. Goulding, H. A. Thiessen, and C. L. Morris, Phys. Rev. C **24**, 598 (1981).
[25] W. B. Cottingame and D. B. Holtkamp, Phys. Rev. Lett. **45**, 1828 (1980).
[26] D. S. Oakley, P. D. Kunz, and C. L. Morris, Phys. Rev. C **41**, 1081 (1990).
[27] J. Heisenberg, J. Lichtenstadt, C. N. Papanicolas, and J. S. McCarthy, Phys. Rev. C **25**, 2292 (1982).
[28] J. Decharge, M. Girod, D. Gogny, and B. Grammaticos, Nucl. Phys. **A358**, 203 (1981); J. Decharge (private communication).
[29] G. R. Satchler, J. Math. Phys. **13**, 1118 (1972).
[30] J. Arvieux, J. P. Albanese, J. Bolger, E. Boschitz, C. H. Q. Ingram, L. Pflug, J. Jansen, J. Zichy, E. Rost, and A. S. Rosenthal, Nucl. Phys. **A312**, 368 (1978).
[31] D. F. Geesaman, C. Olmer, B. Zeidman, R. L. Boudrie, G. S. Blanpied, M. J. Devereux, G. R. Burleson, R. E. Segel, L. W. Swenson, and H. A. Thiessen, Phys. Rev. C **23**, 2635 (1981).
[32] V. Corcalciuc, H. Rebel, R. Pesl, and H. J. Gils, J. Phys. G. **9**, 177 (1983).
[33] I. Hamamoto, Phys. Lett. **66B**, 410 (1977); (private communication).
[34] B. Karaoglu and E. J. Moniz, Phys. Rev. C **33**, 974 (1986).
[35] M. Hirata, F. Lenz, and K. Yazaki, Ann. Phys. (N. Y.) **108**, 116 (1977); M. Hirata, J. H. Koch, F. Lenz, and E. J. Moniz, *ibid.* **120**, 205 (1979).
[36] Y. Horikawa, M. Thies, and F. Lenz, Nucl. Phys. **A345**, 386 (1980).
[37] F. Lenz, M. Thies, and Y. Horikawa, Ann. Phys. (N. Y.) **140**, 266 (1982).
[38] J. H. Koch, E. J. Moniz, and N. Ohtsuka, Ann. Phys. (N. Y.) **154**, 99 (1984); J. H. Koch and E. J. Moniz, Phys. Rev. C **27**, 751 (1983).
[39] A. K. Kerman, H. McManus, and R. M. Thaler, Ann. Phys. (N.Y.) **8**, 551 (1959).
[40] D. J. Ernst and M. B. Johnson, Phys. Lett. B **237**, 164 (1990).
[41] F. Cannata, J. P. Dedonder, and W. R. Gibbs, Phys. Rev. C **41**, 1637 (1990).
[42] R. H. Landau and F. Tabakin, Phys. Rev. D **5**, 2746 (1972).
[43] N. Austern and J. S. Blair, Ann. Phys. (N.Y.) **33**, 15 (1965).
[44] G. E. Brown, A. Sethi, and N. M. Hintz, Phys. Rev. C **44**, 2653 (1991).
[45] G. E. Brown, C. B. Dover, P. B. Siegel, and W. Weise, Phys. Rev. Lett. **60**, 2723 (1988).